Journal of Materials Chemistry A

Polydopamine/Hydroxyapatite Nanowires-based Bilayered Membrane for Photothermal-driven Membrane Distillation

Journal:	*Journal of Materials Chemistry A*
Manuscript ID	TA-ART-11-2019-012703.R1
Article Type:	Paper
Date Submitted by the Author:	22-Jan-2020
Complete List of Authors:	Cao, Sisi; Washington University in Saint Louis, Department of Mechanical Engineering and Materials Science Wu, Xuanhao; Washington University in Saint Louis, Energy, Environmental & Chemical Engineering Zhu, Yaguang; Washington University in Saint Louis, Energy, Environmental and Chemical Engineering Gupta, Rohit; Washington university in st.Louis, Mechanical Engineering Tan, Albern; Washington University, Department of Energy, Environmental and Chemical Engineering Wang, Zhongyang; Washington University in Saint Louis, Energy, Environmental and Chemical Engineering Jun, Young-Shin; Washington University, Energy, Environment and Chemical Engnieering Singamaneni, Srikanth; Washington University, Department of Mechanical Aerospace and Structural Engineering

Polydopamine/Hydroxyapatite Nanowires-based Bilayered Membrane for Photothermal-driven Membrane Distillation

Sisi Cao,[1] Xuanhao Wu,[2] Yaguang Zhu,[2] Rohit Gupta,[1] Albern Tan,[2] Zhongyang Wang,[2] Young-Shin Jun[2]* Srikanth Singamaneni[1]*

[1]*Department of Mechanical Engineering and Materials Science, Institute of Materials Science and Engineering, Washington University in St. Louis, St Louis, MO, 63130, USA*

[2]*Department of Energy, Environmental and Chemical Engineering, Washington University in St. Louis, St. Louis, MO, 63130, USA*

Abstract

In developing countries and resource-limited regions, where no power infrastructure or waste heat from industrial plants is available, photothermal-driven membrane distillation (PMD) has been recognized as an attractive and sustainable technology for freshwater generation. PMD enables easy water collection, inherent fouling resistance, low-pressure operation, and high-salinity water treatment. Hydroxyapatite (HA) nanowires with excellent mechanical flexibility owing to their high aspect ratio, low thermal conductivity, easy surface modification and scalable production offer great potential for highly efficient membrane distillation. Herein, we demonstrate that the environmental-benign HA nanowires-based bilayered film offers the highest photothermal efficiency (62%) and water flux (0.89 $kg \cdot m^{-2} \cdot h^{-1}$) with 1-sun irradiation (1 $kW \cdot m^{-2}$), among the exiting PMD systems without auxiliary heating or multilayer heat recovery reported so far. The hierarchical porous structure formed by the remarkably flexible and intertwined HA nanowires allows low resistance to vapor transport, which is critical for high water flux. Simultaneously, the low thermal conductivity of the thermal insulator layer comprised of HA nanowires prevents conductive heat transfer across membrane, which significantly enhances the thermal efficiency of the membrane. The completely biocompatible, scalable, and thermally-engineered bilayered film demonstrated here achieves highly efficient PMD.

*To whom correspondence should be addressed: singamaneni@wustl.edu (SS) and ysjun@wustl.edu (YJ).

Introduction

Although 71% of earth surface is covered with water, more than 97% of it is saltwater, and freshwater is limited to only about 2.5%.[1] The water crisis has been exacerbated due to environmental pollution, increased agriculture needs, socio-economic development, and population growth.[2, 3] Among various desalination technologies, membrane distillation (MD) has gained wide attention due to its ability to treat highly saline water utilizing waste heat from industrial processes.[4-9] The MD process can be carried out at a lower pressure compared to reverse osmosis (RO) and at a lower temperature than conventional thermal distillation technology.[10-12] In MD system, the hot feed saline water and cold distillate are present on opposite sides of a porous hydrophobic membrane.[13] Driven by the vapor-pressure gradient caused by the temperature difference, the steam, generated at the interface of membrane and hot feed water, transports across the membrane to the cold distillate side, where condensation occurs.[14] However, the implementation of conventional MD is hindered in remote regions and disaster-struck communities where low-grade thermal energy from industrial plants and electricity are not readily available.

To address this problem, photothermal-driven membrane distillation (PMD), where MD is integrated with photothermal materials that can effectively convert light to thermal energy, is being proposed.[15-18] In particular, harnessing the abundant sunlight as a source of thermal energy offers great potential to propel it to developing countries and rural communities. Another merit for PMD is the high thermal efficiency compared to the conventional MD process.[19-21] For conventional MD, the conductive heat transfer across the membrane leads to temperature polarization, eventually impairing desalination efficiency.[22, 23] Localized surface heating can be achieved on photothermal membranes,[24] which remarkably alleviates the temperature polarization and results in higher thermal efficiency.

Most of the photothermal membranes reported to date employ synthetic polymers, such as polypropylene (PP),[25] polytetrafluoroethylene (PTFE)[26, 27] and polyvinylidene fluoride (PVDF),[28-31] as substrates, which are non-biocompatible and non-biodegradable. The disposal of these materials poses a great threat to the environment and ecosystems.[32] Preparation of these membranes *via* precursor polymer powders generally involves toxic organic solvents.[15, 33, 34] Moreover, incorporation of solar absorbers on surface of these synthetic polymers is not straightforward. To assist the loading of the solar absorbers, the inert surfaces of polymer substrates have been coated with binder materials with sticky functional groups.[23] These concerns associated with utilizing synthetic polymer-based membranes highlight the need to

transition to environmentally-benign membrane materials and to develop simple and green processes for PMD.

As a major inorganic mineral in bone and tooth of vertebrates, hydroxyapatite ($Ca_{10}(PO_4)_6(OH)_2$, HA) is well-known for its biocompatibility, biodegradability, and abundance.[35, 36] HA nanowires with a high aspect ratio of length to diameter (> 100) exhibit remarkable mechanical flexibility,[37] and they can be assembled into a flexible film by simple vacuum filtration. The film possesses an interconnected porous network and allows facile transfer of vapor across the film.[38] Owing to their low thermal conductivity, HA nanowires-based films have been employed as thermal insulators in solar steam generators to enhance localized surface heating.[39] Moreover, the hydrophilicity/hydrophobicity of the HA nanowires can be readily tuned by harnessing hydrogen bonding *via* hydroxyl groups or electrostatic interaction *via* charged moieties (*e.g.*, Ca^{2+} ions), which enable facile surface modification.[40, 41] For those reasons, we posit that the biocompatibility, mechanical flexibility, low thermal conductivity, easy processability, and facile surface modification of HA nanowires make them as a promising material platform to realize high-performance photothermal membranes for PMD.

Herein, we introduce a highly efficient bilayered photothermal membrane based on HA nanowires with low resistance for vapor transport and high resistance for heat transfer. For this bilayered structure, the top layer comprises polydopamine (PDA)-coated HA (HA@PDA) nanowires to effectively convert solar energy to heat and a bottom layer comprises chitosan (CS)-bonded HA nanowires (HA-CS) as a thermal insulator (Figure 1). The CS in the bottom layer serves as a bio-degradable molecular glue. The hierarchical structure formed by the highly flexible and intertwined HA nanowires provides a network of channels for facile vapor transport. In addition, the easy surface modification and large surface area of HA nanowires allow dense coating of PDA that is a highly biocompatible and biodegradable solar absorber.[42-44] More importantly, the HA nanowires with low thermal conductivity can significantly reduce the conductive heat transfer across the membranes and increase the thermal efficiency in PMD. Although bilayered structures have been applied in PMD, the importance of a thermal insulator has not been well studied. Our work represents the first detailed study elucidating the role of thermal insulation layer in achieving high photothermal efficiency in PMD. This completely environmentally-friendly bilayered photothermal film exhibits outstanding light absorption, heat insulation, stability, and porosity, leading to high thermal efficiency in PMD. This work illuminates the great potential of HA nanowires in constructing a high-performance and environmentally-friendly photothermal membrane *via* a simple and green processing method.

Results and Discussion

The PDA/HA nanowires bilayered film was fabricated by sequential vacuum filtration of HA-CS and HA@PDA nanowires (Figure 1). The fabrication process is fast and scalable compared to freeze-drying and physical/chemical vapor deposition. HA nanowires were synthesized by a previously reported calcium oleate precursor *via* hydrothermal method, and large-scale synthesis (with a volume up to 100 L) could be achieved using a large stainless-steel autoclave.[41] HA nanowires with diameter of around 20 nm and high aspect ratio (>100) exhibited remarkable flexibility (Figure 2A, B). After dispersing in water, a stable wool-like suspension was observed (inset of Figure 2A). CS, a biopolymer that enables strong interfacial interaction (*e.g.*, hydrogen bonding and electrostatic interaction) with the nanowires, is added to improve the mechanical stability for the HA-CS film.[37]

To fabricate the HA-CS film (thermal insulation layer), the mixture of HA nanowires suspension with 10% (w/w) CS was vacuum filtered. The as-prepared pristine HA-CS film was white (Figure 2D) and the intertwined nanowires formed an interconnected porous network (Figure 2E). The pore size of HA-CS film was analyzed by flow capillary porometry and the mean diameter for pores was found to be around 200 nm (Figure 3A). Thermogravimetric analysis (TGA) showed that the loading of CS was around 4% (w/w) for the pristine HA-CS film (Figure 3B), which was found to be an optimal loading amount for a stable HA-CS film. In contrast, the film fabricated using a mixture of HA nanowires suspension with 5% (w/w) CS could not be successfully peeled from the filter membrane as they broke and disintegrated during the peeling process, suggesting that the HA nanowires are not firmly bound together (Figure S1). Higher loading of CS is also detrimental to the PMD performance as it compromises the porosity of the film. Therefore, the optimal loading of CS, which serves as the binding material, is important to ensure mechanical stability of the film and high PMD performance.

In this work, photothermally-active PDA was used as the solar absorber, because of its excellent biocompatibility, biodegradability, broadband light absorption and high light-to-heat conversion efficiency.[16, 45] To obtain PDA coating, HA nanowires were dispersed in the 10 mM Tris-HCl solution (pH = 8.5) followed by the addition of dopamine. PDA was formed *via* oxidative self-polymerization of dopamine and the reaction was stopped after 24 hours. The coating resulted in a color change of HA nanowires suspension from white (inset of Figure 2A) to dark brown (inset of Figure 2F). Transmission electron microscope (TEM) images revealed the ultrathin PDA coating on the HA nanowires surface, and the surface became significantly rougher (Figure 2G) than the pristine HA nanowires (Figure 2B). The successful coating was confirmed by the

PDA nanotubes obtained after dissolving the HA nanowire cores by HCl, and the thickness for the PDA shell was found to be around 15 nm (Figure S2A). The isoelectric point (pH_{iep}) of pristine HA nanowires was around 2.3, whereas that of HA@PDA suspension was around 4, which is similar to pure PDA and PDA coated surfaces,[46, 47] indicating the successful coating of PDA on HA nanowires (Figure S2B).

To validate the importance of incorporating HA-CS layer as a thermal insulator in PMD, a HA@PDA film with same thickness, consisting of only a solar absorber layer without a thermal insulating layer (HA-CS layer), was fabricated as a comparison. The HA@PDA film was obtained by vacuum filtering the HA@PDA nanowires. In stark contrast with the white color of pristine HA-CS film (Figure 2C), the HA@PDA film was dark brown (Figure 2H). The interconnected pores were also observed for the HA@PDA film, with mean diameter of 230 nm (Figure 3A). Based on TGA analysis, the weight percentage for PDA in the HA@PDA film was around 20% (Figure 3B), which was achieved by 24-hours oxidative self-polymerization of dopamine on HA nanowires. It is important to note that the PDA loading efficiency achieved here is much higher than reported in the case of hydrophilic PVDF film (9.7%) after seven polymerization cycles (each cycle for 24 hours).[16] The difference is ascribed to the much larger surface area of HA nanowires compared to the porous PVDF membrane. HA nanowires were dispersed in the dopamine solution and provided a significantly larger surface for *in situ* PDA coating compared to PVDF membrane. Considering that adequate PDA loading is critical for effective light absorption and solar energy harvesting, HA nanowires offer a unique advantage as templates for PDA loading.

To obtain the bilayered HA-CS/HA@PDA film, HA@PDA nanowires were vacuum-filtered on the surface of HA-CS film (Figure 1). The color of upper layer (Figure 2K) and bottom layer (Figure 2L) of the as-prepared hybrid film was the same as HA@PDA film and HA-CS film, respectively, which confirmed the bilayered structure. Owing to the mechanical flexibility of the HA nanowires, HA-CS film, HA@PDA film, and the bilayered films could be easily bent without inducing brittle fracture (Figure 2D, I, M). A nacre-like multilayered structure was observed in the cross-section of bilayered film (Figure 2N-O) and HA@PDA film (Figure S3A-B), resulting from the physical and chemical interactions between the nanowires (*e.g.*, physical entanglements, hydration forces, van der Waals interaction, hydrogen bonding and electrostatic interaction).[40] These available pores and interlayer spacings in the films will provide sufficient channels for effective vapor transport during the PMD operation.

Considering that the heat transfer resistance of the membrane plays a key role in the thermal efficiency of MD, we investigated the thermal conductivity of HA@PDA film and HA-CS

film, which constitute the top and bottom layers of the hybrid film, respectively. The measurements were conducted according to our previously reported method.[48] The film was sandwiched between two glass slides, with the top glass slide in contact with ice and the bottom one in contact with a hot plate, which was employed as heat source to establish heat flow (the temperature was increased from 70 °C to 120 °C with an interval of 10 °C). The temperature gradient along cross-section film was monitored by an infrared camera (insets of Figure 3C-D). The thermal conductivity for HA-CS film was measured to be 0.048 $W•K^{-1}•m^{-1}$ (Figure 3C), which is comparable to the widely used thermal insulator materials for interfacial heating systems, such as polystyrene foam (0.040 $W•K^{-1}•m^{-1}$).[49] On the other hand, the HA@PDA film exhibited a thermal conductivity of 0.147 $W•K^{-1}•m^{-1}$ (Figure 3D), which is three times higher than the HA-CS film. The low thermal conductivity of HA-CS film makes it as an excellent thermal insulator. Under light illumination, the thermal energy is generated in HA@PDA layer at the top and the HA-CS film at the bottom reduces the conductive heat transfer across the membrane. Therefore, the enhanced heat localization enabled by including the thermal insulator can significantly reduce the temperature polarization, which offers a higher driving force for vapor transport across the membrane and greatly improves the thermal efficiency of the photothermal membrane.

The hydrophobicity of membrane is critical for MD process.[8, 50-52] For hydrophobic microporous membranes, only vapor can to diffuse across the membrane, whereas mass transfer of liquid phase is prevented. Although as-prepared HA nanowires are highly hydrophilic, their facile surface modification allows easy hydrophobization. The films were subjected to fluorosilanization using (tridecafluoro-1,1,2,2-tetrahydrooctyl)-trichlorosilane (FTCS) to obtain a hydrophobic surface.[53] SEM images confirmed that the porous network was not affected by FTCS treatment (Figure S5), and contact angle measurement indicated the successful hydrophobic modification. The original surfaces of HA-CS film (Figure S4A), HA@PDA film (Figure S4B) and bilayered films (Figure S4C-D) were hydrophilic with water contact angles of 0°, following hydrophobization, the contact angles were 120°, 130°, and 126°, respectively (insets of Figure S5).

To investigate the light absorption of and HA@PDA/HA-CS film, the optical transmittance and reflectance of HA-CS, HA@PDA and HA@PDA/HA-CS film after FTCS treatment are measured and compared (with the film thickness ~70 μm) (Figure 4A-B). The pristine HA-CS film exhibited high transmittance (~33.3%) and reflectance (~46.2%) in the visible region, implying relatively small light extinction (~20.5%). On the other hand, the HA@PDA film exhibited extremely low light transmittance (~0%) and reflectance (~2.5%), which translated into a large

extinction (~97.5%). The difference in optical properties is associated with the presence of PDA, which is known to exhibit broadband light absorption. In addition, the interconnected porous structure of the film causes the multiple reflection within the film, enabling high light absorption.[54] Owing to the presence the HA@PDA layer at the top, the bilayered film also displayed very low light transmittance (~0%) and reflectance (~2.3%), which corresponds to a high light extinction (~97.7%). The bilayer structure of the membrane does not affect the optical properties. Hence, the large optical absorption and excellent light-to-heat conversion efficiency enabled by PDA makes the bilayered film a promising membrane for PMD.

Now, we turn our attention to the photothermal conversion efficiency of these films, which critically determines their thermal efficiency for PMD operation. The surface temperature of films in open air was measured using an infrared camera, under simulated solar light illumination at a power density of 1 kW•m^{-2} (1 sun) and 9 kW•m^{-2} (9 sun) (Figure 4C). After light irradiation for 120 seconds, the surface temperature for pristine HA-CS film increased from ~25 °C to ~28 °C at 1-sun irradiation and to ~32 °C at 9-sun irradiation, while the temperature increased to ~43 °C at 1-sun and to ~238 °C at 9-sun illumination for HA@PDA film (Figure 4D-E). In the presence of the HA-CS as a thermal insulator layer, the surface temperature of bilayered film increased to ~46 °C at 1-sun irradiation and ~245 °C at 9-sun irradiation. The higher surface temperatures for the bilayered structures, compared to the pure HA@PDA film in the open air, highlights the importance of integrating a thermal insulating layer into the photothermal membrane, which effectively mitigates the heat dissipation and enhances the localized heating at the surface.

The PMD performance of HA@PDA/HA-CS bilayered film was evaluated in a specially designed direct contact membrane distillation (DCMD) module (Figure S6), with a HA@PDA film with the same thickness as a control for comparison (Figure 5A). The PMD setup was maintained to be same as our reported test condition.[16] Simulated seawater, 0.5 M NaCl solution at ambient temperature (20 °C), was used as the feed water. Because the feed water flow rate can affect the water collection as we showed in our previous work,[16] the flow rate was fixed at 3.6 ml•min^{-1}, based on our previous work. The distillate at room temperature with a flow rate of 16.2 ml•min^{-1} was circulated on the opposite side of the membrane, and the generated freshwater was quantified by measuring the weight increase of the distillate as a function of irradiation time (Figure 5C) (all tests were conducted for 60 minutes). The water flux for HA@PDA film was 0.65 kg•m^{-2}•h^{-1} and 6.16 kg•m^{-2}•h^{-1} under 1-sun and 9-sun illumination, respectively. On the other hand, for the HA@PDA/HA-CS bilayered film, the water flux was found to be 0.89 kg•m^{-2}•h^{-1} and 8.28 kg•m^{-2}•h^{-1} under 1-sun and 9-sun irradiation, respectively. These results indicated that the presence of a

thermal insulation layer led to ~27% and ~34% higher water flux compared to the HA@PDA film under 1-sun and 9-sun illumination, respectively.

The thermal efficiency of photothermal membrane is determined by the ratio of heat flux required to generate distillate flux to the total irradiated solar flux, $\eta = \frac{\dot{m}h_{vap}}{I}$, where $\dot{m}$ represents the distillate flux of water, h_{vap} refers to the total evaporation enthalpy change, and I is the total incident solar flux. Given the water evaporation enthalpy of 2454 kJ•kg^{-1} (~ 0.68 kW•kg^{-1}•h),[23, 55] the water flux was 0.65 kg•m^{-2}•h^{-1} for HA@PDA film under 1 sun illumination, so the minimum heat flux needed to sustain this distillate flux is 0.45 kW•m^{-2} for HA@PDA film. The total incident solar flux is 1 kW•m^{-2}, so the corresponding thermal efficiency of HA@PDA film is 45%. The distillate flux of HA@PDA film was 6.16 kg•m^{-2}•h^{-1} under 9-sun illumination, so the required minimum heat flux is 4.20 kW•m^{-2} and the calculated thermal efficiency is 46%. This efficiency is much higher than the previously reported efficiency achieved by carbon black nanoparticles-coated PVDF membrane (~22%). The superior performance is closely related with the high loading of PDA and hierarchical porous network of the membrane. The large surface area and facile surface modification of HA nanowires allow dense and stable coating of PDA, resulting in high thermal energy output from HA@PDA nanowires under light irradiation. Furthermore, the nanowires with high aspect ratio intertwine with each other and form the interconnected porous structure, which results in a low resistance for vapor transport. As for the carbon black nanoparticles-loaded PVDF membrane, polymeric binder is added to prevent the desorption and leaching of the light-absorbing nanoparticles from the porous matrix, which inevitably narrows the pores and reduce the mass transport.[23, 56]

Under identical test conditions, we also evaluated the performance of HA@PDA/HA-CS bilayered film. The efficiency reached 62% and 63% under 1-sun and 9-sun irradiation, respectively, which is much higher than the HA@PDA film and previously reported PDA-coated PVDF membrane (~45%).[16] This bilayered membrane represents the highest efficiency for PMD among those reported so far, treating the saline water at room temperature without auxiliary heating or heat recovery system.[16, 23] The improvement is mainly attributed to the enhanced localized heating at the evaporative surface owing to the presence of the HA-CS thermal insulation layer. Membranes with a high thermal efficiency have a relatively high resistance to conductive heat transfer as well as low resistance to mass transfer.[57] The low thermal conductivity of HA-CS layer in the hybrid film significantly reduces the conductive heat dissipation across the membrane and remarkably impairs the temperature polarization, yielding much stronger driving force for vapor transport.

During PMD, the thermal energy generated by the PDA leads to surface heating, so that the temperature of membrane surface (T_1) is larger than that of feed water (T_f). The generated vapor on the hot surface transfers to the cold distillate side due to the temperature difference between two sides of the membrane ($T_1>T_2$). However, the conductive heat transfer across the membrane results in the temperature increase on the permeate side of membrane (Figure 5B). The smaller temperature difference across the membrane eventually lowers driving force for the vapor transfer. In the presence of HA-CS layer as a thermal insulator, the conductive heat from the hot surface (T_3) to the permeate side (T_4) of membrane can be greatly reduced (Figure 5B). Hence, more thermal energy is preserved on the surface for localized heating, and thus a larger temperature difference across the membrane is achieved with the bilayered film, ultimately resulting in higher solar efficiency for PMD.

To evaluate the long-term PMD performance, the HA@PDA film and bilayered film were tested over 5 cycles (each cycle for 1 hour). The average fluxes of the HA@PDA film were 0.63 $kg•m^{-2}•h^{-1}$ and 5.83 $kg•m^{-2}•h^{-1}$, and those of HA@PDA/HA-CS film were 0.89 $kg•m^{-2}•h^{-1}$ and 8.13 $kg•m^{-2}•h^{-1}$, under 1-sun and 9-sun illumination, respectively (Figure 5D). The average thermal efficiencies of HA@PDA film were 43% and 44%, and those of bilayered film were 61% and 62%, under 1-sun and 9-sun illumination, respectively (Figure 5E). The performance using both films remained constant during the 5 cycles, and the variations in flux and thermal efficiency were less than 5%. As mentioned above, the anti-wetting property of membranes is critical for MD process. Therefore, the durability of hydrophobic modification of the membrane has also been investigated. The contact angle of HA@PDA film before PMD test was 129° and it was 125° for the bilayered film after 5-cycles testing (Figure S7). The negligible change (variation less than 5%) in the contact angle of the films indicates the durability of hydrophobic modification over repeated use of the membranes. Based on the Cantor–Laplace equation,[58, 59] the calculated liquid entry pressure for HA@PDA film and bilayered film is 110 kPa and 100 kPa, respectively. We then evaluated the mechanical stability of the film. Even after the vigorous mechanical agitation for 2 weeks, the bilayered film did not display any signs of disintegration (Figure S8A), and no change in morphology and hydrophobicity was observed (Figure S8B, S8C), highlighting the potential for long-term PMD application. This excellent durability of the membrane is ascribed to the outstanding mechanical properties (*e.g.*, high flexibility) of HA nanowires and the intertwined morphology of the network, which serves as mechanical interlocks. In fact, numerous reports in the past demonstrated that the strong interfacial interactions (*e.g.*, hydrogen bonding and electrostatic interactions) of HA nanowires with materials possessing polar functional groups (*e.g.* glass fiber, cellulose fiber, and CS) provides excellent mechanical strength of HA nanowires-

based films, which can be used as printing papers,[36] separators for lithium battery,[38] bone-fracture fixation materials,[37] and fire-alarm wallpapers.[35] Considering the excellent mechanical stability, low thermal conductivity, interconnected porous network, facile surface modification, scalable synthesis and environmentally-benign nature, HA nanowire-based membranes are highly comparable to, if not better than, conventional materials for membrane distillation, such as PVDF, PTFE and PP.

Conclusions

Here, we have successfully designed and fabricated a biocompatible HA@PDA/HA-CS bilayered film membrane for highly efficient PMD. The photothermal efficiency of the PDA/HA nanowires film reached 62% under 1-sun illumination and represents the highest efficiency for PMD reported so far for treating saline water at room temperature without any auxiliary heating system or heat recovery system. The facile surface modification and large surface area make HA nanowires an outstanding template for forming a dense, stable, and efficient PDA coating, which in turn ensures broadband light absorption and high light-to-heat conversion. More importantly, the interconnected porous structure, formed by the highly flexible and intertwined nanowires, leads to low resistance to vapor transfer. Simultaneously, the low thermal conductivity of HA nanowires layer significantly reduces the conductive heat transfer from the evaporative surface to the cold permeate side. This further improved the localized heating and vapor transfer across the membrane. In the presence of HA nanowires layer as a thermal insulator, the water flux of bilayered film is ~27% (under 1 sun) and ~34% (under 9 sun) higher than those of the HA@PDA film under identical test condition, respectively. Furthermore, the excellent mechanical robustness of bilayered film contributes to long-term and stable PMD performance, showing great potential for real-world application. This environmentally-benign, highly efficient and mechanically stable HA nanowires-based photothermal membrane is highly promising for freshwater generation in the remote regions and disaster-struck communities by utilizing the abundantly available sunlight and saline water.

Experimental methods

Preparation of hydroxyapatite (HA) nanowires

HA nanowires were synthesized by the calcium oleate precursor solvothermal method reported previously.[41] For all experiments, unless otherwise mentioned, we have used deionized water (≥ 18.2 MΩ-cm, Barnstead). Briefly, sodium hydroxide (NaOH, Sigma Aldrich) aqueous solution (1.73 M, 56.3 ml), calcium chloride ($CaCl_2$, Sigma Aldrich) aqueous solution (250 mM, 45 ml), and

sodium dihydrogen phosphate dihydrate (NaH_2PO_4•$2H_2O$, Alfa Aesar) aqueous solution (333 mM, 67.5 ml) were added to the mixture of H_2O (50.6 ml), methanol (22.5 ml) (Sigma Aldrich), and oleic acid (35.1 g) (Sigma Aldrich) under stirring, respectively. Then, the mixture was transferred to a Teflon-lined stainless-steel autoclave (Parr Co., Moline, IL) and maintained at 180 ˚C for 24 h. The precipitates were centrifuged at 1500 rpm for 5 min and the supernatant was decanted. The collected product was dispersed in the mixture of ethanol (95%, Sigma Aldrich) and deionized water with volume ratio of 1 to 1. The mixture was centrifuged at 1500 rpm for 5 min, and the supernatant was subsequently removed. This wash step was repeated for three times. Finally, the products were dispersed in deionized water and the supernatant was decanted after centrifuging at 4000 rpm for 5 min. The rinsing step was repeated for three times and the final products were dispersed in deionized water. To determine the HA concentration, the HA suspension (1 ml) was dried in the 70 °C oven for overnight, and the weight of dry HA was measured.

Preparation of polydopamine (PDA)-coated HA (HA@PDA) nanowires

To ensure the uniform dispersion of HA nanowires in solution, HA nanowires (20 mg) were dispersed in Tris-HCl buffer solution (10 mM, pH = 8.5, 50 ml) followed by sonication for 1 min. Then dopamine (20 mg, Sigma Aldrich) was added to the above suspension, followed by stirring for 24 h in open air to get the homogeneous PDA coating on HA nanowires. Finally, the resultant products were collected, and to remove the salt and PDA nanoparticles, they were washed with deionized water for three times by centrifuging at 6000 rpm for 5 min. The collected products were dispersed in deionized water.

Preparation of HA-CS film, HA@PDA film, and HA@PDA/HA-CS bilayered film

The chitosan (CS) powders (200 mg, Sigma Aldrich) were dispersed in the acetic acid (Sigma Aldrich) aqueous solution (1% v/v, 10 ml), and the mixture was kept in an oil bath at 60 ˚C for 2 h under stirring to obtain a homogenous solution. CS solution (20 mg/ml, 111 µl) was added to HA nanowires suspension (1 mg/ml, 20 ml), and the mixture was left on a rotating mixer for 10 min to ensure uniform coatings of CS on the HA nanowires. The mixture of CS and HA was homogenous, and no aggregation was observed. Then, the mixture was vacuum-filtered through hydrophilic polypropylene (PP) membrane (diameter = 90 mm, pore size = 0.45 µm, Cole-Parmer) to fabricate the HA-CS film. Once all water passed through the filter, the film was dried at 60 ˚C for 10 min. The HA-CS film was obtained by peeling from the membrane filter.

The HA@PDA film was also obtained by vacuum-filtering HA@PDA nanowires suspension (20 mg) on PP membrane. To obtain the HA@PDA/HA-CS bilayered film, the above mixture (10 ml) of HA nanowires and CS was vacuum-filtered on PP membrane. Once all water passed through the filter, the HA@PDA nanowires suspension (1 mg/ml, 10 ml) was vacuum-filtered on the top surface of HA-CS film. The film was dried at 60 ˚C for 10 min and finally the HA@PDA/HA-CS bilayered film was peeled from the membrane filter.

In both membrane preparation, the peeling process does not affect the mechanical strength.

Preparation of PDA hollow nanowires

HCl solution (1M, Sigma Aldrich) was used to dissolve the HA nanowires from the core of the HA@PDA nanowires. After adding HCl solution to HA@PDA nanowires suspension, the mixture was vortexed for 5 s and then washed with deionized water for three times by centrifuging at 6000 rpm for 10 min. The collected the products were dispersed in deionized water.

FTCS treatment

To obtain the hydrophobic surface, the obtained films were treated with (tridecafluoro-1,1,2,2-tetrahydrooctyl)-trichlorosilane (Sigma Aldrich) vapor in a sealed container at 70 ˚C for 24 h. Then, to confirm the hydrophobic surface modification after FTCS treatment, water contact angle of films was measured using a contact angle analyzer (Phoenix 300, Surface Electro Optics Co. Ltd).

Nano-/Micro-structure characterization

SEM images of the surface and the cross section of the films and the nanowires were obtained after sputter coating the samples with gold. FEI Nova 2300 field-emission scanning electron microscope (SEM) was used at an acceleration voltage of 10.5 kV. The transmission electron microscope (TEM) images of nanowires were obtain using JEOL JEM-2100F field emission microscopy. Thermogravimetric analysis (TGA) was performed using TA Instruments Q5000 IR Thermogravimetric Analyzer in nitrogen gas flow (at rate of 10 °C•min^{-1}). The pore size distribution of films was measured by a CFP-LEP-1100A capillary flow porometer. Zeta potential measurements were performed using a Zetasizer Nano ZS (ZEN3600) dynamic light scattering system (Malvern Instruments).

Thermal conductivity measurement

The thermal conductivities of HA-CS film and HA@PDA film were measured by monitoring the temperature distributions across the thickness of films that were sandwiched between two glass

microscope slides. The bottom glass slide was in contact with a hot plate and the top glass slide was in contact with ice. The temperature of hot plate was increased from 70 °C to 120 °C, in steps of 10 °C. The vertical temperature distribution for the sandwich was monitored by a high-speed IR camera (Telops FAST M3k). The emissivity coefficient of a glass slide and a sample was assumed to be 0.9 to obtain the temperature distribution.[42] Fourier equation was used to calculate the thermal conductivity of each sample:

$$q' = K\frac{\Delta T}{\Delta X}$$

The heat flux (q') was calculated by assuming the thermal conductivity (K) of 1.05 $W \cdot m^{-1} \cdot K^{-1}$ for glass slides. Because the glass slide and samples experience the same heat flux, the heat flux value obtained for glass slide was used to measure the thermal conductivity for HA-CS film and HA@PDA film samples, respectively.

Optical properties and photothermal performance measurement

Reflectance and transmittance spectra of films were obtained using a CRAIC micro spectrophotometer (QDI 302) coupled to a Leica optical microscope (DM 4000M) with 20x objective in the range of 450–800 nm with 10 accumulations and 100 ms exposure time in reflection and transmission mode, respectively. The surface temperature of films was monitored by an IR camera (Ti 100, FLUKE) under light illumination using a solar simulator (Newport 66921 Arc Lamp) under both unfocused irradiation (1 sun) and focused irradiation (9 sun).

Photothermal-driven membrane distillation performance measurement

The PMD performance was evaluated using a direct contact membrane distillation (DCMD) module. The PMD cell was constructed using acrylonitrile butadiene styrene (ABS) plastic by 3D printing. The diameter for MD cell was 1.5 cm. A Teflon substrate with thickness of 1 mm was placed between the feed side and distillate side to support the photothermal membrane. The 0.5 M NaCl aqueous solution was chosen to simulate the seawater as the feed water and deionized water was chosen as distillate stream at the bottom of the membrane, both of which were at room temperature (20 °C). The feed and distillated water were continuously circulated using two peristaltic pumps (Welco WPX1-F1 and Stenner 85MHP5), with a flow rate of 3.6 $ml \cdot min^{-1}$ and 16.2 $ml \cdot min^{-1}$, respectively. The thickness of feed water was maintained at 8 mm. The collected permeate water was recorded using a weight scale (Sartorius ELT402) to measure the weight of the distillate reservoir every 2 min. The light illumination to DCMD was achieved using a solar simulator (Newport 66921 Arc Lamp) under both 1 and 9 sun illumination.

Mechanical agitation

The HA@PDA/HA@-CS film (1 cm x 1 cm, L x W) was placed in a 50 ml test tube filled with water, then it was subjected to rigorous mechanical agitation a tube rotator (VWR Multimix Tube Rotator Mixer 13916-822) for 2 weeks.

Liquid entry pressure calculation

The liquid entry pressure of HA@PDA and HA@PDA/HA-CS film was calculated based on the Cantor–Laplace equation.[58, 60]

$$LEP = \frac{-2B\gamma_L Cos\theta}{r_{max}}$$

where LEP was the liquid entry pressure of pure water in Pa, B represented a dimensionless geometrical factor that includes the irregularities of the pores (B = 1 for assumed cylindrical pores), γ_L referred the liquid surface tension in N•m^{-1} (in this case water at 20°C, 0.07286 N•m^{-1}), θ represented the contact angle in degree, and r_{max} was the maximal pore radius in m (non-closed pore, r_{max} = 0.86 x 10^{-6} m according to the measurement of flow capillary porometry).

Conflicts of interest

There are no conflicts to declare.

Acknowledgements

We acknowledge the support from National Science Foundation Environmental Engineering Program (CBET-1604542). The authors thank the Nano Research Facility (NRF) and Institute for Materials Science and Engineering (IMSE) at Washington University in St.Louis for providing access to characterization facilities. The authors thank Prof. Vijay Ramani of Environmental and Chemical Engineering at Washington University in St. Louis for providing the vacuum filtration setups, and Prof. Xianfeng Wang of Donghua University for providing the capillary flow porometer to characterize the pore size distribution of films.

Figures

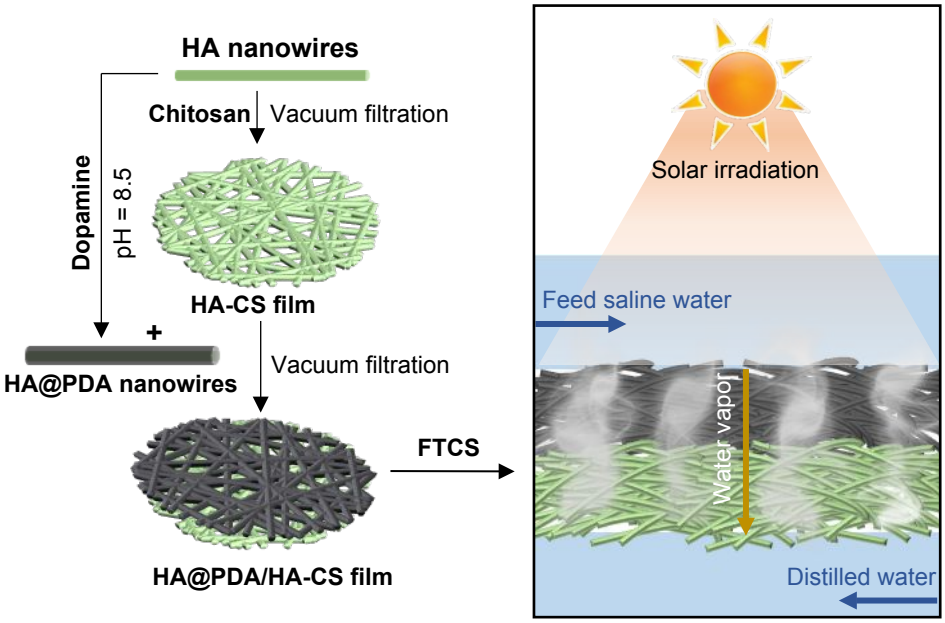

Figure 1. Schematic illustration depicting the fabrication of HA@PDA/HA-CS bilayered photothermal film and PMD based on this bilayered structure. Chitosan (CS) is added to the HA nanowires suspension and subsequently the mixture is vacuum filtered to prepare the HA-CS film. HA nanowires are dispersed in the dopamine solution (pH = 8.5) to allow the PDA coating on the HA surface and the obtained HA@PDA nanowires were vacuum filtered onto the HA-CS film to prepare the bilayer photothermal film. Finally, to obtain hydrophobic surface, the film was fluorosilanized using (tridecafluoro-1,1,2,2-tetrahydrooctyl)-trichlorosilane (FTCS). PMD was conducted using a direct contact membrane distillation cell under simulated solar irradiation.

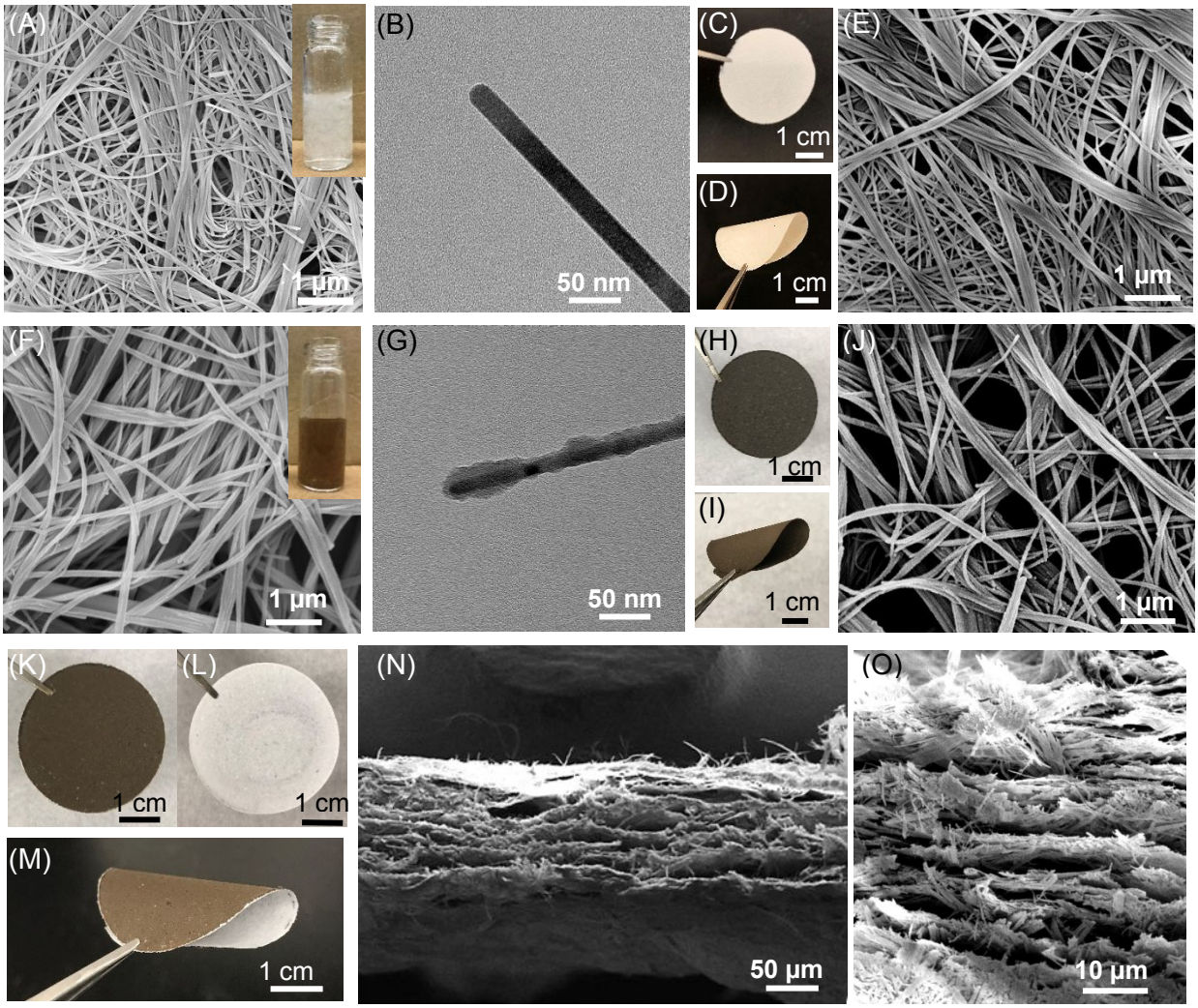

Figure 2. (A) SEM image of HA nanowires (inset shows the photograph of HA nanowires suspension). (B) TEM image of HA nanowires. Photograph of a flat (C) and deformed (D) HA-CS film. (E) SEM image of the HA-CS film. (F) SEM image of HA@PDA nanowires (inset shows the photograph of HA@PDA nanowire suspension). (G) TEM image of HA@PDA nanowires. Photograph of a flat (H) and deformed (I) HA@PDA film. (J) SEM image of the HA@PDA film. Photograph of top (K), bottom (L) of HA@PDA/HA-CS film and a deformed bilayered film (M). The cross-section SEM images of the HA@PDA/HA-CS film in low magnification (N) and high magnification (O).

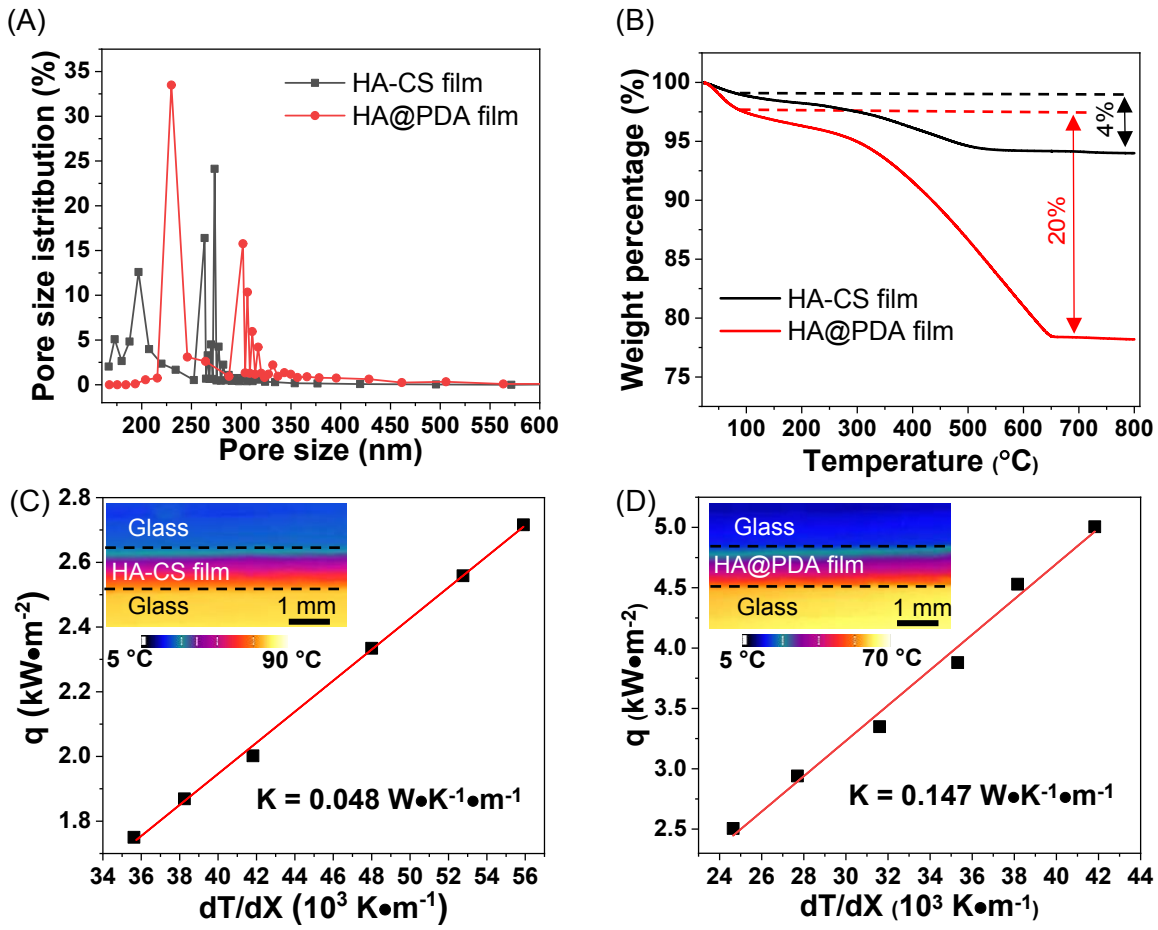

Figure 3. Characterization of HA-CS film and HA@PDA film. Pore size distributions (A) and TGA analyses (B) of representative HA-CS film and HA@PDA film. Thermal conductivity of HA-CS film (C) and HA@PDA film (D). Insets: representative IR images showing the temperature gradient along the thickness of the HA-CS film (C) and HA@PDA film (D).

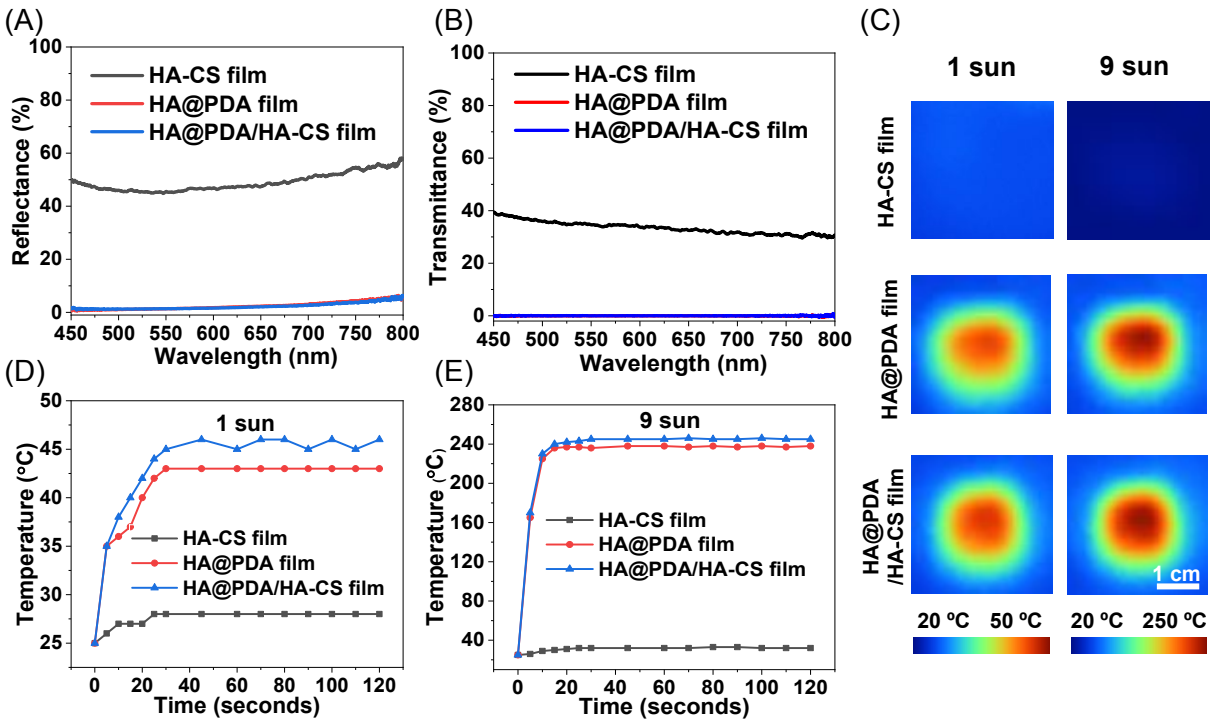

Figure 4. Optical and photothermal properties of the membranes. Reflectance (A) and transmittance spectra (B) of the HA-CS film, HA@PDA film, and HA@PDA/HA-CS film. (C) IR images showing the surface temperature of the HA-CS film, HA@PDA film and HA@PDA/HA-CS film under 1-sun and 9-sun illumination in open air after 120 seconds. The plots showing the surface temperature of the HA-CS film, HA@PDA film and HA@PDA/HA-CS film under 1-sun (D) and 9-sun illumination (E) as a function of irradiation time.

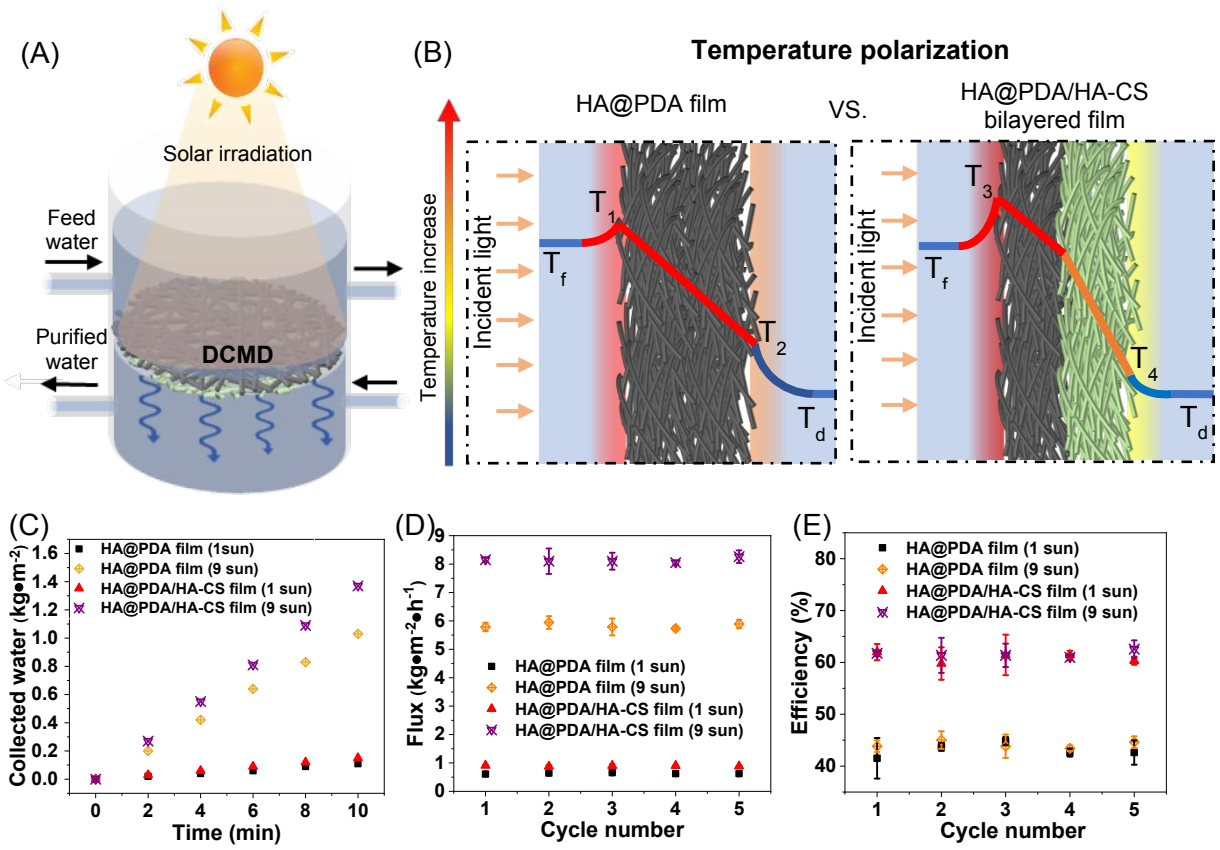

Figure 5. PMD performance for the HA@PDA film and HA@PDA/HA-CS film. (A) Schematic illustration of photothermal direct contact membrane distillation (DCMD) using HA@PDA/HA-CS film with thickness of the feed water at 8 mm. (B) Schematic illustration of thermal profile of DCMD using a HA@PDA film (left) and HA@PDA/HA-CS film (right) under solar irradiation. (C) PMD performance of HA@PDA film and HA@PDA/HA-CS film in purifying 0.5 M NaCl saline water under 1-sun and 9-sun illumination. Flux (D) and thermal efficiency (E) of the photothermal DCMD system using the HA@PDA film and HA@PDA/HA-CS film, with 0.5 M NaCl saline water under 1-sun and 9-sun irradiation for 5-cycles testing (each cycle for 1 hour, standard deviation obtained from measurements of 3 samples; some of error bars were hidden by the symbols because the error bars are smaller than symbol sizes).

References

1. D. Ghim, Q. Jiang, S. Cao, S. Singamaneni and Y.-S. Jun, *Nano Energy*, 2018, **53**, 949-957.
2. *The United Nations world water development report 2019: Leaving No One Behind*, 2019.
3. Q. Jiang, D. Ghim, S. Cao, S. Tadepalli, K.-K. Liu, H. Kwon, J. Luan, Y. Min, Y.-S. Jun and S. Singamaneni, *Environmental Science & Technology*, 2019, **53**, 412-421.
4. C. Boo and M. Elimelech, *Nature nanotechnology*, 2017, **12**, 501.
5. P. Goh, T. Matsuura, A. Ismail and N. Hilal, *Desalination*, 2016, **391**, 43-60.
6. E. H. Ang, Y. Z. Tan and J. W. Chew, *Journal of Materials Chemistry A*, 2019, **7**, 10206-10211.
7. A. Deshmukh, C. Boo, V. Karanikola, S. Lin, A. P. Straub, T. Tong, D. M. Warsinger and M. Elimelech, *Energy & Environmental Science*, 2018, **11**, 1177-1196.
8. R. Long, X. Lai, Z. Liu and W. Liu, *Energy*, 2018, **148**, 1060-1068.
9. Z. Wang, T. Horseman, A. P. Straub, N. Y. Yip, D. Li, M. Elimelech and S. Lin, *Science Advances*, 2019, **5**, eaax0763.
10. K. W. Lawson and D. R. Lloyd, *Journal of membrane Science*, 1997, **124**, 1-25.
11. A. Alkhudhiri, N. Darwish and N. Hilal, *Desalination*, 2012, **287**, 2-18.
12. T. Y. Cath, V. D. Adams and A. E. Childress, *Journal of Membrane Science*, 2004, **228**, 5-16.
13. L. Camacho, L. Dumée, J. Zhang, J.-d. Li, M. Duke, J. Gomez and S. Gray, *Water*, 2013, **5**, 94-196.
14. M. Gryta, *Membranes*, 2012, **2**, 415-429.
15. A. Politano, P. Argurio, G. Di Profio, V. Sanna, A. Cupolillo, S. Chakraborty, H. A. Arafat and E. Curcio, *Advanced Materials*, 2017, **29**, 1603504.
16. X. Wu, Q. Jiang, D. Ghim, S. Singamaneni and Y.-S. Jun, *Journal of Materials Chemistry A*, 2018, **6**, 18799-18807.
17. Y.-S. Jun, X. Wu, D. Ghim, Q. Jiang, S. Cao and S. Singamaneni, *Accounts of Chemical Research*, 2019, **52**, 1215-1225.
18. E. Chiavazzo, M. Morciano, F. Viglino, M. Fasano and P. Asinari, *Nature Sustainability*, 2018, **1**, 763-772.
19. Y.-S. Jun, D. Ghim, X. Wu, S. Cao and S. Singamaneni, *HDIAC Journal*, 2019, **6**, 6.
20. S. Cao, Q. Jiang, X. Wu, D. Ghim, H. Gholami Derami, P.-I. Chou, Y.-S. Jun and S. Singamaneni, *Journal of Materials Chemistry A*, 2019.
21. W. Wang, Y. Shi, C. Zhang, S. Hong, L. Shi, J. Chang, R. Li, Y. Jin, C. Ong, S. Zhuo and P. Wang, *Nature Communications*, 2019, **10**, 3012.
22. A. Politano, G. Di Profio, E. Fontananova, V. Sanna, A. Cupolillo and E. Curcio, *Desalination*, 2019, **451**, 192-199.
23. P. D. Dongare, A. Alabastri, S. Pedersen, K. R. Zodrow, N. J. Hogan, O. Neumann, J. Wu, T. Wang, A. Deshmukh, M. Elimelech, Q. Li, P. Nordlander and N. J. Halas, *Proceedings of the National Academy of Sciences*, 2017, **114**, 6936-6941.
24. X. Han, W. Wang, K. Zuo, L. Chen, L. Yuan, J. Liang, Q. Li, P. M. Ajayan, Y. Zhao and J. Lou, *Nano Energy*, 2019, **60**, 567-575.
25. Y. Shao, M. Han, Y. Wang, G. Li, W. Xiao, X. Li, X. Wu, X. Ruan, X. Yan and G. He, *Journal of membrane science*, 2019, **579**, 240-252.
26. S. Tadepalli, H. Hamper, S. H. Park, S. Cao, R. R. Naik and S. Singamaneni, *ACS Biomaterials Science & Engineering*, 2016, **2**, 1084-1092.
27. L. Huang, J. Pei, H. Jiang and X. Hu, *Desalination*, 2018, **442**, 1-7.
28. Y. Liao, R. Wang and A. G. Fane, *Environmental science & technology*, 2014, **48**, 6335-6341.

29. T. Chen, A. Soroush and M. S. Rahaman, *Industrial & Engineering Chemistry Research*, 2018, **57**, 14535-14543.
30. Y. Z. Tan, H. Wang, L. Han, M. B. Tanis-Kanbur, M. V. Pranav and J. W. Chew, *Journal of Membrane Science*, 2018, **565**, 254-265.
31. L. Han, Y. Z. Tan, C. Xu, T. Xiao, T. A. Trinh and J. W. Chew, *Journal of Membrane Science*, 2019, **588**, 117196.
32. D. Hou, T. Li, X. Chen, S. He, J. Dai, S. A. Mofid, D. Hou, A. Iddya, D. Jassby, R. Yang, L. Hu and Z. J. Ren, *Science Advances*, 2019, **5**, eaaw3203.
33. H. Ye, X. Li, L. Deng, P. Li, T. Zhang, X. Wang and B. S. Hsiao, *Industrial & Engineering Chemistry Research*, 2019, **58**, 3269-3281.
34. Q. Huang, S. Gao, Y. Huang, M. Zhang and C. Xiao, *Journal of Membrane Science*, 2019, **582**, 203-210.
35. F.-F. Chen, Y.-J. Zhu, F. Chen, L.-Y. Dong, R.-L. Yang and Z.-C. Xiong, *ACS nano*, 2018, **12**, 3159-3171.
36. B. Q. Lu, Y. J. Zhu and F. Chen, *Chemistry–A European Journal*, 2014, **20**, 1242-1246.
37. T. W. Sun, Y. J. Zhu and F. Chen, *Chemistry–A European Journal*, 2017, **23**, 3850-3862.
38. H. Li, D. Wu, J. Wu, L. Y. Dong, Y. J. Zhu and X. Hu, *Advanced Materials*, 2017, **29**, 1703548.
39. D.-D. Qin, Y.-J. Zhu, F.-F. Chen, R.-L. Yang and Z.-C. Xiong, *Carbon*, 2019, **150**, 233-243.
40. F.-F. Chen, Y.-J. Zhu, Z.-C. Xiong, T.-W. Sun and Y.-Q. Shen, *ACS applied materials & interfaces*, 2016, **8**, 34715-34724.
41. Z. C. Xiong, Y. J. Zhu, D. D. Qin, F. F. Chen and R. L. Yang, *Small*, 2018, **14**, 1803387.
42. Q. Jiang, H. G. Derami, D. Ghim, S. Cao, Y.-S. Jun and S. Singamaneni, *Journal of Materials Chemistry A*, 2017, **5**, 18397-18402.
43. L. Zong, M. Li and C. Li, *Nano energy*, 2018, **50**, 308-315.
44. X. Wu, G. Y. Chen, W. Zhang, X. Liu and H. Xu, *Advanced Sustainable Systems*, 2017, **1**, 1700046.
45. H. Gholami Derami, Q. Jiang, D. Ghim, S. Cao, Y. J. Chandar, J. J. Morrissey, Y.-S. Jun and S. Singamaneni, *ACS Applied Nano Materials*, 2019, **2**, 1092-1101.
46. J. Feng, H. Fan, D.-a. Zha, L. Wang and Z. Jin, *Langmuir*, 2016, **32**, 10377-10386.
47. G. Pérez-Mitta, J. S. Tuninetti, W. Knoll, C. Trautmann, M. E. Toimil-Molares and O. Azzaroni, *Journal of the American Chemical Society*, 2015, **137**, 6011-6017.
48. Q. Jiang, L. Tian, K. K. Liu, S. Tadepalli, R. Raliya, P. Biswas, R. R. Naik and S. Singamaneni, *Advanced Materials*, 2016, **28**, 9400-9407.
49. H. Ghasemi, G. Ni, A. M. Marconnet, J. Loomis, S. Yerci, N. Miljkovic and G. Chen, *Nature communications*, 2014, **5**, 4449.
50. H. Chamani, T. Matsuura, D. Rana and C. Q. Lan, *Journal of membrane science*, 2019, **572**, 332-342.
51. C. Li, X. Li, X. Du, T. Tong, T. Y. Cath and J. Lee, *ACS Applied Materials & Interfaces*, 2019, **11**, 18456-18465.
52. M. Sun, C. Boo, W. Shi, J. Rolf, E. Shaulsky, W. Cheng, D. L. Plata, J. Qu and M. Elimelech, *Advanced Functional Materials*, 2019, **29**, 1903125.
53. M. E. Leitch, C. Li, O. Ikkala, M. S. Mauter and G. V. Lowry, *Environmental Science & Technology Letters*, 2016, **3**, 85-91.
54. P. Wang, *Environmental Science: Nano*, 2018, **5**, 1078-1089.
55. F. Woodward and J. Sheehy, *Principles and measurements in environmental biology*, Elsevier, 2017.
56. J. Wu, K. R. Zodrow, P. B. Szemraj and Q. Li, *Journal of Materials Chemistry A*, 2017, **5**, 23712-23719.
57. X. An, G. Xu, B. Xie and Y. Hu, *Journal of Materials Chemistry A*, 2019, **7**, 2376-2384.

58. S. S. Ray, S.-S. Chen, C. T. Ngoc Dan, H.-T. Hsu, H.-M. Chang, N. C. Nguyen and H.-T. Nguyen, *RSC Advances*, 2018, **8**, 1808-1819.
59. A. Franken, J. Nolten, M. Mulder, D. Bargeman and C. Smolders, *Journal of Membrane Science*, 1987, **33**, 315-328.
60. A. C. M. Franken, J. A. M. Nolten, M. H. V. Mulder, D. Bargeman and C. A. Smolders, *Journal of Membrane Science*, 1987, **33**, 315-328.